



Impact of river discharge on phytoplankton bloom dynamics in eutrophic estuaries: A model study

Bo Liu ^{*}, Huib E. de Swart

Institute for Marine and Atmospheric Research Utrecht, Utrecht University, Utrecht, The Netherlands



ARTICLE INFO

Article history:

Received 18 December 2014

Received in revised form 16 July 2015

Accepted 26 July 2015

Available online 7 August 2015

Keywords:

Phytoplankton bloom

River flow

Flushing

Idealised model

ABSTRACT

Field observations in estuaries reveal that phytoplankton blooms are strongly affected by advection processes related to river flow. To gain quantitative insight into this dependence, experiments were performed with a new idealised model that couples physical and biological processes. Advection of phytoplankton and nutrient by subtidal flow was explicitly accounted for, as well as longitudinal and vertical mixing processes. Results show that the idealised model is capable of reproducing the observed bloom. The specific spatial distribution of phytoplankton population emerges because the latter is suppressed in the upper reach by the advection processes, and the growth is limited in the lower reach by low nutrient concentrations. A sensitivity study of model results to different river discharges reveals the presence of three regimes. In the low discharge regime, blooms form because growth is faster than decay due to advection processes. In the high discharge regime, the situation is opposite and no blooms form. If time scales of growth and advection are comparable (in moderate discharge regime), phytoplankton population increases significantly slower compared to the low discharge regime. Results of additional model runs, in which water depth and the e-folding length scale of estuarine width convergence were varied, revealed that the three regimes occur in all these cases.

© 2015 Elsevier B.V. All rights reserved.

1. Introduction

Phytoplankton play a major role in the biogeochemical cycle of estuaries. Their blooms, which are defined as the events of rapid production and accumulation of phytoplankton biomass (Cloern, 1996), have attracted much attention due to their notable impact on estuarine ecological health. Temporal and spatial characteristics of blooms are tightly regulated by estuarine physical processes (Cloern, 1996; Cloern et al., 2014; Golubkov, 2009).

River discharge, as a main forcing agent for the estuarine circulation, has been linked to phytoplankton blooms by extensive field studies (for instance, Sin et al., 1999; Howarth et al., 2000; Maier et al., 2012; Peierls et al., 2012). However, the relationship between the two has been found to be complex. Using a conceptual model, Lucas et al. (2009) revealed that the phytoplankton growth-loss balance determines whether phytoplankton biomass increases with, decreases with, or is insensitive to transport time. In their study, the transport time scale was quantified in terms of a flushing time, residence time or transit time. However, this conceptual model could not describe detailed temporal or spatial variability and the model outcomes are sensitive to values of its input parameters.

Numerical modelling has also been widely applied to explain the observed correlation between river inflow and phytoplankton production. Flushing has been demonstrated to be a key factor for the development and location of estuarine blooms by earlier studies, for instance, Lucas et al. (1998, 1999) and Zakardjian et al. (2000). These studies also suggested that advective flux is a main reason for the critical depth theory of Sverdrup (1953) to fail in forecasting blooms in many shallow waters. This theory states that a bloom commences when the depth of the surface mixed layer becomes less than the critical depth (that is the depth above which the averaged production is balanced by the loss). Using a coupled physical–biochemical model, Arndt et al. (2007) attributed the high phytoplankton production during low river discharge in the Scheldt estuary to multiple favourable effects that result from low river inflow: high residence time, low suspended sediment concentration and low water volume in the upper reach. Azevedo et al. (2014) applied a 3D model to the Douro estuary and reproduced the observed parabolic relationship between phytoplankton biomass and river flow magnitude, with biomass reaching a maximum for moderate river discharges and decreasing for both increased and decreased river flow. They inferred that this relationship was caused by the decreased nutrient and biomass input for low river inflow and the low residence times for high river flow.

Models like those in the studies cited above can reproduce the reality fairly well. Nevertheless, their results are often difficult to interpret since the variability of phytoplankton production is a consequence of changes in all the physical processes included in the model. Cloern

^{*} Corresponding author at: Institute for Marine and Atmospheric Research Utrecht, Utrecht University, Princetonplein 5, 3584 CC Utrecht, The Netherlands. Tel.: +31 302537759.

E-mail address: B.Liu2@uu.nl (B. Liu).

et al. (2014) pointed out that the variability of river inflow drives the variability of other processes, such as advective and diffusive transport, nutrient supply, sediment transport, formation of density stratification, where each of these processes has its own impact on phytoplankton biomass accumulation and/or production.

Thus, to obtain further insight into the relation between phytoplankton biomass and river flow, it is helpful to study the effect of individual physical processes on phytoplankton bloom dynamics. For this aim, analytical/semi-analytical models are suitable tools. De Swart et al. (2009) constructed an analytical model, with which they demonstrated the dependence of phytoplankton growth pattern on spatial variations in turbidity and in nutrients that results from sub-tidal flow. However, their model can only be applied to study the onset of blooms and excludes the advection and horizontal mixing.

With the aim towards a further understanding of regulation of blooms by river discharge, this study is focused on quantifying the role of advective and mixing processes related to river flow on bloom formation. The Taw estuary (SW England) was chosen as the prototype estuary, where a strong link between intensity and spatial variability of blooms and river discharge was reported by Maier et al. (2012). The research aim is specified as follows:

- 1) To demonstrate the importance of flushing of phytoplankton by river flow in formation of observed blooms in eutrophic estuaries;
- 2) To quantify the dependence of the key characteristics in phytoplankton bloom dynamics on the magnitude of river discharge.

As an extension of the model of De Swart et al. (2009), an idealised model was developed to achieve these research aims. This new model allows for long-term evolution and explicitly includes advective and longitudinal mixing processes. The equations governing biological as well as the hydrodynamic processes are introduced in Section 2. In Section 3, the results for the experiments simulating the observed bloom are shown, and the results of sensitivity of phytoplankton bloom dynamics to river discharge are presented. These results are further analysed in Section 4, where influence of water depth, e-folding length scale of estuarine width convergence is also discussed. Conclusions are given in Section 5.

2. Methodology

2.1. Model design and domain

The model in this study was constructed in modular forms. Phytoplankton and nutrient dynamics were included in the biological module, which was coupled to a hydrodynamic module that governs sub-tidal flow. A simple turbulence closure scheme was adopted. The longitudinal (along-channel) advection and mixing processes were explicitly accounted for in the biological module in the current study. As a result of this extension, the biological module can only be solved numerically.

A simplified geometry of the estuary considered in this study is illustrated in Fig. 1. A Cartesian coordinate system is chosen with the x -axis pointing from river head ($x = 0$) to the mouth ($x = L$) and the z -axis from the water surface ($z = 0$) downward to the bottom ($z = H$). The water depth (H) is assumed constant. The estuarine width is modelled as

$$b(x) = b_0 \exp\left(\frac{x}{L_b}\right), \quad (1)$$

with b_0 the width at the river head, and L_b the e -folding length of width convergence.

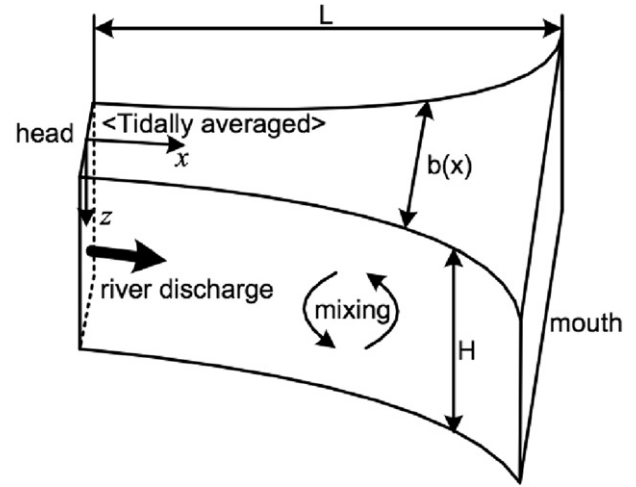


Fig. 1. The configuration of the idealised estuary in the model. Here, L is the length of the estuary, H is the constant water depth, and $b(x)$ is the width which is modelled with Eq. (1).

2.2. Biological module

The governing equation for phytoplankton and nutrient dynamics are

$$\frac{\partial P}{\partial t} = \mu(N, I)P - mP - v \frac{\partial P}{\partial z} - w \frac{\partial P}{\partial z} - u \frac{\partial P}{\partial x} + \frac{\partial}{\partial z} \left(\kappa_v \frac{\partial P}{\partial z} \right) + \frac{1}{b} \frac{\partial}{\partial x} \left(b \kappa_h \frac{\partial P}{\partial x} \right), \quad (2)$$

$$\frac{\partial N}{\partial t} = -\alpha \mu(N, I)P + \epsilon \alpha mP - w \frac{\partial N}{\partial z} - u \frac{\partial N}{\partial x} + \frac{\partial}{\partial z} \left(\kappa_v \frac{\partial N}{\partial z} \right) + \frac{1}{b} \frac{\partial}{\partial x} \left(b \kappa_h \frac{\partial N}{\partial x} \right). \quad (3)$$

Here, $P = P(x, z, t)$ denotes the width-averaged phytoplankton population density (cells m^{-3}) and $N = N(x, z, t)$ is the width-averaged nutrient concentration (mmol m^{-3}). The specific growth rate of phytoplankton $\mu(N, I)$ is constrained by the nutrient concentration and light intensity (I). Furthermore, m is the specific loss rate of phytoplankton that accounts for respiration and zooplankton grazing, v is the sinking velocity of phytoplankton due to gravity, α is the nutrient amount in each phytoplankton cell and ϵ is the proportion of respired/grazed phytoplankton that is subsequently recycled. Finally, u and w are the along-channel and vertical velocity, and κ_h and κ_v are longitudinal and vertical turbulent diffusivity coefficient, respectively.

The parameterisation for the specific growth rate follows Huisman et al. (2006):

$$\mu(N, I) = \mu_{\max} \min\left(\frac{N}{H_N + N}, \frac{I}{H_I + I}\right). \quad (4)$$

In this expression, μ_{\max} is the maximum specific growth rate, H_N and H_I are the half-saturation constants for nutrient-limited and light-limited growth, respectively, and \min denotes the minimum function.

The light is supplied at the water surface and its intensity decreases exponentially with depth according to Lambert–Beer's law:

$$I = I_{in} \exp\left(-k_{bg}z - k_{phyto} \int_0^z P(t, \theta) d\theta\right). \quad (5)$$

Here, I_{in} is the incident light intensity, k_{bg} the background turbidity and k_{phyto} the specific light absorption coefficient by phytoplankton. The last integral term represents the 'shading effect' of phytoplankton.

The corresponding boundary conditions read

$$\left(vP - \kappa_v \frac{\partial P}{\partial z} \right) \Big|_{surf,b} = 0, \quad \left(\kappa_v \frac{\partial N}{\partial z} \right) \Big|_{surf,b} = 0, \quad (6)$$

$$\left(uP - \kappa_h \frac{\partial P}{\partial x} \right) \Big|_r = 0, \quad N|_r = N_{river}, \quad (7)$$

$$P|_s = P_{sea}, \quad N|_s = N_{sea}. \quad (8)$$

The subscripts *surf*, *b*, *r* and *s* refer to the surface, the bottom, the river head and the sea mouth, respectively. At the surface and the bottom, zero-flux boundary conditions are applied for both phytoplankton and nutrient (Eq. (6)). At the riverine boundary, a zero-flux condition is assumed for phytoplankton, implying no riverine source for phytoplankton and fixed concentration condition is assumed for the nutrient (see Eq. (7)). At the seaward boundary, a fixed population density and fixed concentration are set for phytoplankton and nutrient (see Eq. (8)), respectively.

Compared to the model of De Swart et al. (2009), the new idealised model in this study explicitly accounts for advection and horizontal mixing of phytoplankton and nutrients (i.e. the fourth, fifth and last term in the right hand side of Eqs. (2) and (3)), and the 'shading effect' (the second term in the right hand side of Eq. (5)) as well.

2.3. Hydrodynamic module

The sub-tidal circulation model in Hansen and Rattray (1965) was adapted for the estuary with an exponentially increasing width from river towards sea, as is considered in this study. The width-averaged longitudinal velocity is

$$u(x, z) = \underbrace{\frac{3Q}{2b(x)H} \left(1 - \left(\frac{z}{H} \right)^2 \right)}_{\text{river flow}} + \underbrace{\frac{gH^3\beta}{48\rho_0 A_v} \frac{ds}{dx} \left(1 - 9\left(\frac{z}{H} \right)^2 - 8\left(\frac{z}{H} \right)^3 \right)}_{\text{density-driven flow}}. \quad (9)$$

The first term on the right-hand side describes the flow driven by the fresh water discharge Q , whilst the second term shows the density-driven flow due to the longitudinal salinity gradient ds/dx . In Eq. (9), g is the acceleration due to gravity and A_v is the vertical eddy viscosity coefficient. Furthermore, ρ_0 is a constant reference density and β is the coefficient of isohaline contraction. Following Warner et al. (2005) and Talke et al., (2009), salinity is assumed to be vertically well mixed and modelled as

$$s(x) = \frac{1}{2} s_* \left[1 + \tanh \left(\frac{x - x_c}{x_L} \right) \right]. \quad (10)$$

An analytical shape of the salinity versus distance from the river head is plotted in Fig. 2. In Eq. (10), s_* is the salinity of sea water; x_c is the position where the salinity is $0.5s_*$ and the along-channel salinity gradient reaches its maximum; x_L scales the slope of the salinity gradient and $(x_c - x_L)$ is the position where salinity is $0.12s_*$. In this study, a salt intrusion length was defined as $\chi_L = L - (x_c - x_L)$.

The width-averaged vertical velocity is obtained by solving the continuity equation and it reads

$$w(x, z) = - \int_0^z \left(\frac{\partial u}{\partial x} + \frac{u}{L_b} \right) dz'. \quad (11)$$

Assuming sub-tidal salinity distribution in the estuary is determined by fresh water discharge and the longitudinal diffusivity, the longitudinal turbulent diffusivity κ_h is calculated following Helder and Ruurdij (1982):

$$\kappa_h = \frac{Q s}{H b ds/dx}. \quad (12)$$

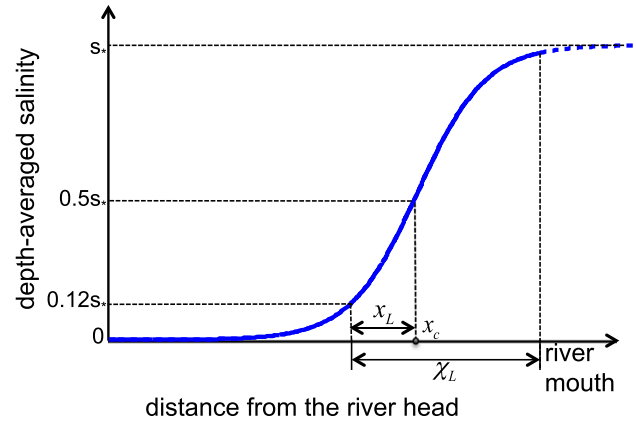


Fig. 2. The analytical shape of depth-averaged salinity versus distance from the river head. Furthermore, s_* is the salinity of sea water, x_c is the location of salinity, x_L is the width of salinity frong and χ_L is salt intrusion length.

The vertical eddy viscosity A_v is taken as constant. Furthermore, assuming that mixing is not affected by stratification, the vertical turbulent diffusivity coefficient $\kappa_v = A_v$ (Munk and Anderson, 1948).

2.4. Model implementation and verification

The biological module contains two coupled nonlinear differential equations and it can not be solved analytically. To obtain numerical solutions of the biological variables P and N , a finite difference method is chosen and central differencing schemes are used for advection, diffusion terms; and a fourth-order Runge–Kutta scheme is used to discretise the time derivatives (Press et al., 1992).

The model was tested by comparing its results with those of the 1D nonlinear model of Huisman et al. (2006) and with those of De Swart et al. (2009), yielding good agreement (see Electronic Supplement 1). Note that the model of Huisman et al. (2006) employs a sophisticated implicit numerical scheme and yields oscillatory and chaotic behaviour of phytoplankton biomass for low vertical mixing in an ocean environment. The new idealised model also captured these oscillations, indicating that the numerical scheme used in this model performs well.

2.5. Experimental setup

As stated in Introduction, the Taw estuary has been chosen as the prototype estuary of this study. The map and location of the Taw estuary are displayed in Fig. 3. Here $x = 0$ and $x = L$ locate at the sampling station A and D, respectively. The geometrical parameters for the Taw estuary were derived from Pethick (2007). The following values were used to model the geometry of the domain: $H = 7$ m, $L = 22.7$ km, $b_0 = 15$ m and $L_b = 5.3$ km. A rectangular grid system was used, with 41×501 grid nodes in vertical and longitudinal direction, respectively. The time step ranged from 2×10^{-5} day to 1×10^{-5} day and it decreased with increasing magnitude of river discharge.

The values of parameters in the biological module are listed in Table 1, which were adopted from other studies (that are cited in the caption of this table). The terms that contain these parameters are highly simplified representatives of complex biological and hydrodynamic processes, hence the choices of the parameter values can potentially influence the results. For this reason, the sensitivity of results to these parameters was also carried out and the outcomes are presented and discussed in the Electronic Supplement 2.

It has been reported that at the river mouth phytoplankton population density shows relatively low values compared to that of the interior of an estuary (Corbett, 2010; Maier et al., 2012). During a

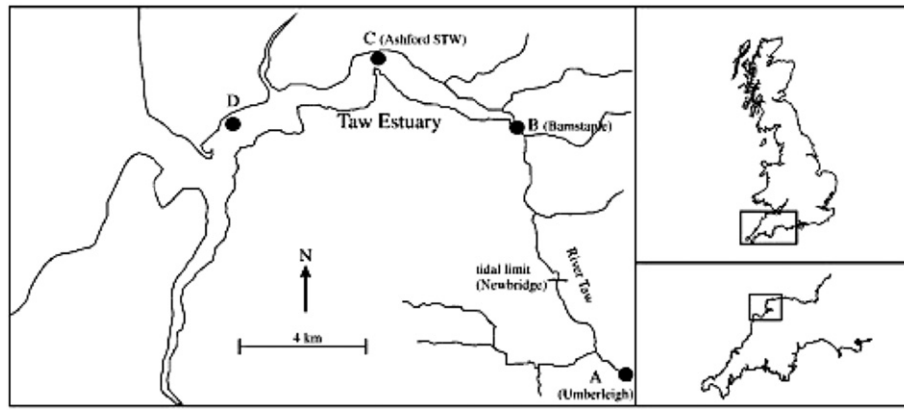


Fig. 3. The left panel displays the map of the Taw estuary and the right panels show its location, reprised from Maier et al. (2012). The full circles A–D represent the sampling sites.

phytoplankton bloom, population density typically increases by a factor of $10^2 - 10^3$, and the typical peak population density is in order of $10^8 - 10^{11}$ cells m^{-3} (Dugdale et al., 2012; Hall et al., 2013). Hence, the seawater population density P_{sea} was set to 10^7 cells m^{-3} . The limiting nutrient is phosphorus according to Maier et al. (2012). Often the nutrient concentration at the river mouth appears low as well (Corbett, 2010; Maier et al., 2012), and the river inflow is the main nutrient source for estuaries (Conley, 2000; Maier et al., 2012). Thus, N_{sea} and N_{river} were estimated as 0.25 and 2.5 mmol m^{-3} with the field data of Maier et al. (2012), respectively.

Phytoplankton distribution in the initial state was assumed longitudinal uniform. The vertical distribution of P was calculated from $vP - \kappa_v \partial P / \partial z = 0$, subject to the constraint $(1/H) \int_0^H P dz = P_0$. Here, P_0 was set to the same value as P_{sea} . The initial nutrient distribution was determined by conducting runs with the model in which phytoplankton were absent.

The reference density and the coefficient of isohaline contraction in Eq. (9) are $\rho_0 = 10^3$ kg m^{-3} and $\beta = 0.83$ kg m^{-3} psu $^{-1}$. The along-channel salinity distribution depends on the freshwater inflow (Diez-Minguito et al., 2013; Monismith et al., 2002). Subsequently, smooth continuous relationships between x_L , x_C , which determine the salinity profile, and Q were constructed from data. The seawater salinity was taken as $s_* = 34$ psu (Maier et al., 2012). First, the values for x_C and x_L for different measured discharge amounts were obtained by fitting the data of Maier et al. (2012) to Eq. (10). Next, a power law regression between intrusion length x_L and Q was used, following Monismith et al. (2002) and Diez-Minguito et al. (2013):

$$x_L = aQ^{-b}. \quad (13)$$

Using the data of x_C and x_L for each Q , the fitting parameters were determined: $a = 20$ km, $b = 0.3$. The value of b falls in the typical range reported by Hansen and Rattray (1965). A similar regression was assumed for x_C :

$$x_C = cQ^{-d}. \quad (14)$$

The best fit resulted in $c = 15$ km, $d = 0.5$. Thus, with the fitting curves (Eqs. (13) and (14)), the salinity profile (Eq. (10)) was determined for any river discharge. The residual flow and the longitudinal turbulent diffusivity coefficient follow from Eqs. (1) and (9)–(12). The vertical eddy viscosity and turbulent diffusivity were taken as 6×10^{-3} m 2 s $^{-1}$.

To achieve the first research aim (to demonstrate the importance of flushing of phytoplankton by river flow in formation of observed blooms in eutrophic estuaries), two experiments were carried out. One with a river discharge $Q = 10$ m 3 s $^{-1}$ and the other with the the river-driven flow (the first term on the right-hand side of Eq. (9)) being switched off. Note that the only difference between these two experiments is that the river-driven flow component is eliminated, however, the density-driven flow and mixing are kept the same. The used value of Q is a representative value for the discharge during the period April 1–April 14 (2008) when a phytoplankton bloom was observed in the Taw estuary. The results will be shown in Section 3.1. As for the sensitivity of phytoplankton bloom dynamics to river discharge (research aim 2), a series of experiments was conducted with different Q (in m 3 s $^{-1}$) imposed at river end boundary, ranging from 4 to 100 m 3 s $^{-1}$. Here not only the river flow, but also the density driven flow and mixing coefficients vary with Q according to Eqs. (9)–(14). These results will be shown in Section 3.2.

Table 1

Biological and abiotic characteristics and parameters for the reference case. Values of these parameters are chosen following the literatures listed below or fall in the typical range presented in these studies.

| Symbol | Interpretation | Units | Value |
|---------------|---|--------------------------------------|-------------------------|
| I_{in} | Incident light intensity | μ mol photons m^{-2} s $^{-1}$ | 400 |
| k_{bg} | Background turbidity | m^{-1} | 0.045 (a) |
| k_{phyto} | Absorption coefficient of phytoplankton | m^2 cell $^{-1}$ | 6×10^{-10} (b) |
| μ_{max} | Maximum specific growth rate | day $^{-1}$ | 0.96 (c) |
| H_I | Half-saturation constant of light-limited growth | μ mol photons m^{-2} s $^{-1}$ | 20 (b) |
| H_N | Half-saturation constant for nutrient-limited growth | mmol nutrient m^{-3} | 0.5 (d,e) |
| m | Specific loss rate | day $^{-1}$ | 0.24 (e) |
| α | Nutrient amount in each phytoplankton cell | mmol nutrient cell $^{-1}$ | 1×10^{-9} (b) |
| ε | The proportion of respired/grazed phytoplankton that is subsequently recycled | Dimensionless | 0.5 (b) |
| v | Settling velocity | m day $^{-1}$ | 1.0 (e) |

Sources are (a) May et al. (2003), (b) Huisman et al. (2006), (c) Popovich and Gayoso (1999), (d) Arndt et al. (2011), and (e) Sarthou et al. (2005).

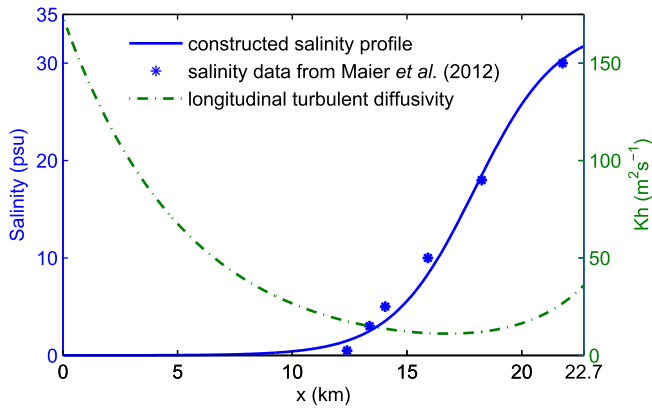


Fig. 4. The blue solid line depicts the along-estuary salinity profile for the reference case, i.e. river discharge $Q = 10 \text{ m}^3 \text{ s}^{-1}$. The blue stars display the salinity data on April 14, 2008 from Maier *et al.* (2012). The dashed green line shows the longitudinal turbulent diffusivity versus the distance from the river head as computed from Eq. (12).

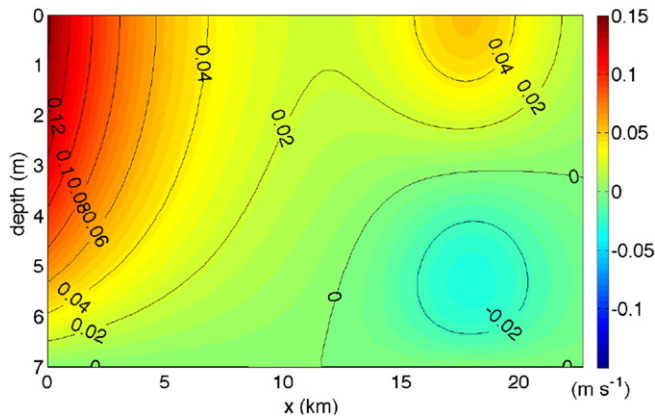


Fig. 5. The width-averaged longitudinal velocity in the estuary for the reference case, in which x is distance from the river head and z is distance to the surface.

3. Results

3.1. Phytoplankton bloom dynamics—reference case

First, the patterns of salinity, longitudinal velocity and longitudinal eddy diffusion coefficient in the reference case are examined. The modelled longitudinal salinity (blue solid line in Fig. 4) agrees well with the observed salinity by Maier *et al.* (2012). The longitudinal turbulent diffusivity (green dashed line in Fig. 4) exhibits a non-monotonic pattern, with a maximum at the river head and a minimum at the location where salinity has its largest along-channel gradient. Fig. 5 shows contour values of the width-averaged along-channel velocity $u(x, z)$ in the estuary. It reveals that in the upper reach ($0 \leq x \leq 7 \text{ km}$) the flow is mainly driven by fresh water discharge, whereas in the lower reach ($x \geq 15 \text{ km}$) the density-driven component significantly contributes to $u(x, z)$.

Fig. 6(a) illustrates the temporal evolution of the domain-integrated phytoplankton population M_P (in cells) and nutrient amount M_N (in mmol). Initially, M_P increases (approximately) exponentially. Here, a inflection time T_i is used to denote this period of exponential growth. In this case, at $T_i = 9$ days, $\partial M_P / \partial t$ reaches its maximum. Since a bloom is often defined as a strong increase in phytoplankton population during a short time, T_i can be interpreted as the time scale of bloom formation. At the end of the third week, M_P reaches a maximum, followed by a slight decrease afterwards. In total, it takes 36 days for the system to reach the non-transient state. Hereafter, this time scale is denoted as the stabilising time T_s . Accordingly, M_N in the estuary decreases with time and it ultimately becomes constant (equilibrium state).

The spatial distribution of the phytoplankton population density at equilibrium is shown in Fig. 6(b). It is characterised by the presence of a bloom and an (almost) uniform distribution in the vertical direction. The near-bottom population density is slightly higher (about 1%) than that at the surface. Since phytoplankton cells sink to the bottom due to gravity and there is no loss for phytoplankton (benthic grazing), cells accumulate near the bottom.

Fig. 7(a) displays the evolution of the near-surface (0.35 m below water surface) population density in the estuary. The reason to select this depth is to facilitate the comparison between model output and field data. Clearly, a bloom commences in the second week and stabilises after three weeks. At first, the location of the along-channel maximum population density (indicated by the white line) quickly shifts from the river head to the middle reach of the estuary. After two weeks, it shifts landwards again. The along-channel maximum

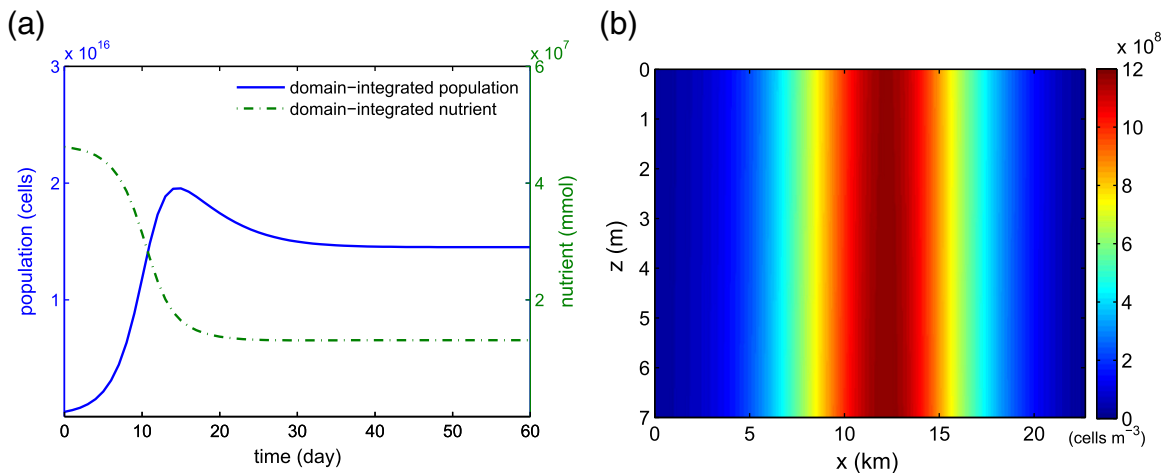


Fig. 6. (a) The domain-integrated total phytoplankton population M_P and nutrient M_N versus time for the reference case. (b) The spatial distribution of phytoplankton population density at equilibrium for the reference case, in which x is distance from the river head and z is distance to the surface.

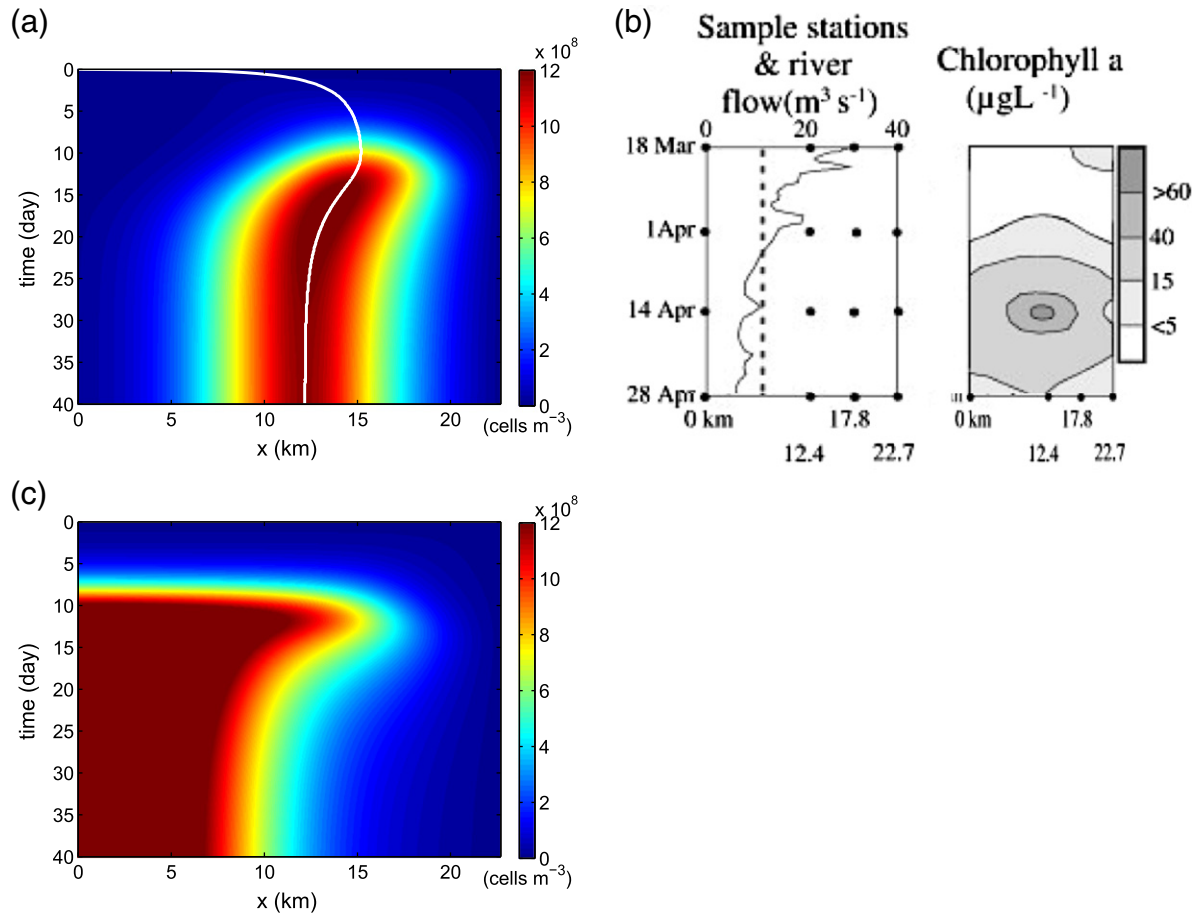


Fig. 7. (a) Contour plot of the near-surface (35 cm under water surface) phytoplankton population density for the reference case as a function of distance x to the river head and time t . The white solid line depicts the location of the along-channel maximum population density. (b) Observations by Maier et al. (2012). The left sub-panel plots river flow for the period of March 18 to April 28 (2008) in the Taw estuary, and the solid circle marks the sampling sites as in Fig. 1(b) (site A, 0 km; site B, 12.4 km; site C, 17.8 km; site D, 22.7 km). The right sub-panel shows the variability of the near-surface chlorophyll a concentration. (c) Contour plot of the near-surface phytoplankton population density for the case where the river-driven flow is switched off, as a function of distance x to the river head and time t .

population density at equilibrium, denoted as P_{\max} , is a factor of 10^2 higher than that of the initial population density.

The modelled phytoplankton bloom behaviour bears many similarities with that observed by Maier et al. (2012) (which is shown in Fig. 7(b)): a bloom commences in the middle reach of the estuary in the course of approximately two weeks. Note that the measurements show chlorophyll a concentration, which is a good indicator of population density when light intensity and temperature are relatively stable (Behrenfeld et al., 2005). A noticeable difference is that the modelled bloom does not fade (as seen in the data) since the river discharge and riverine nutrient source was fixed rather than variable.

Fig. 7(c) shows the evolution of the near-surface population density in the estuary with the river-driven flow being switched off but the density-driven flow and mixing coefficients kept the same. Like the reference case, a bloom forms and the system eventually reaches equilibrium. In contrast, the bloom now occupies the entire upper reach of the estuary. Moreover, the bloom commences earlier and is noticeably more intense compared to the reference case. Clearly, the river flow is essential to form the spatial pattern of the observed bloom, and also influences the magnitude and timing of the bloom.

3.2. Sensitivity of bloom formation to river discharge

As in the previous section, the main characteristics of the results will be presented and discussed with M_p , M_N , P_{\max} , the location of P_{\max} , T_i and T_s . Moreover, a dimensionless ‘river discharge’ \tilde{Q} is defined as the ratio of

flushing rate to maximum net specific growth rate. Table 2 lists the definitions/formulations of these quantities.

In the experiments conducted for different \tilde{Q} , P and N behave qualitatively similarly to that in the reference case. In particular, a steady state is ultimately achieved in each of these experiments. However, their results are quantitatively different. This is visible in Fig. 8(a) that

Table 2

Definition of symbols and terms used to present and discuss results in this study.

| Term | Definition | Formula/specification |
|---------------|--|--|
| Near-surface | 0.35 m below water surface | — |
| $M_p(t)$ | Domain-integrated phytoplankton population | $\int_0^L \int_0^H b P dz dx$ |
| $M_N(t)$ | Domain-integrated nutrient amount | $\int_0^L \int_0^H b N dz dx$ |
| P_{\max} | Near-surface maximum population density at equilibrium, also denoted as bloom intensity | $\max(P _{z=0.35\text{m}})$ |
| T_i | The time at which $\partial M_p / \partial t$ reaches its maximum | The time when $\partial^2 M_p / \partial t^2 = 0$ |
| T_s | The time at which M_p becomes 99% of equilibrium M_p | — |
| \tilde{Q} | The dimensionless river discharge, calculated as the ratio of flushing rate (Q/V) and maximum net growth rate ($\mu_{\max} - m$) | $\tilde{Q} = \frac{Q/V}{\mu_{\max} - m}$ $V = \int_0^L \int_0^H H dx$ |
| \tilde{Q}_l | The dimensionless river discharge for which P_{\max} reaches $90 \times P_{\text{sea}}$ | — |
| \tilde{Q}_h | The dimensionless river discharge for which P_{\max} reaches $2 \times P_{\text{sea}}$ | — |

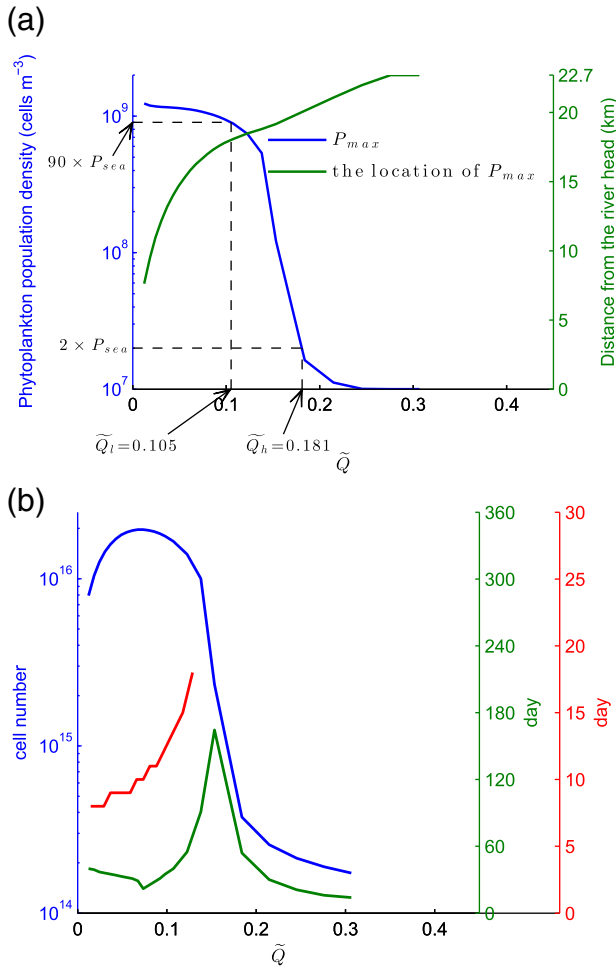


Fig. 8. (a) Blue line depicts bloom intensity P_{max} at equilibrium for different dimensionless river discharges \tilde{Q} . Green line shows the along-channel location of P_{max} . (b) Dependence of domain-integrated phytoplankton population M_p (blue line) at equilibrium, the stabilising time T_s (green line) and the inflection time T_i (red line) on dimensionless river discharges \tilde{Q} .

shows the dependences of bloom intensity P_{max} and its location on \tilde{Q} . As can be seen, P_{max} (the blue line) decreases with \tilde{Q} , which implies phytoplankton bloom weakens and eventually no bloom forms as river discharge increases. Furthermore, \tilde{Q}_l and \tilde{Q}_h are defined as the dimensionless river discharge for which P_{max} reaches 90 and 2 times of the background density P_{sea} , respectively (see Fig. 8(a)). Here, $\tilde{Q}_l = 0.105$ and $\tilde{Q}_h = 0.181$. It is clear that P_{max} decreases faster with increasing \tilde{Q} in the region of moderate discharge conditions ($\tilde{Q}_l \leq \tilde{Q} \leq \tilde{Q}_h$) than that for weak or strong discharges. This implies that the system is more sensitive to river discharge under moderate discharge conditions than under either low discharge ($\tilde{Q} \leq \tilde{Q}_l$) or high discharge ($\tilde{Q} \geq \tilde{Q}_h$) conditions. Meanwhile, the location of P_{max} shifts seawards with increasing \tilde{Q} (the green line).

Fig. 8(b) displays the sensitivity of domain-integrated phytoplankton population M_p in equilibrium (blue line) to \tilde{Q} . Generally, the values of M_p are high for low river discharges and low for high river discharges. In contrast to bloom intensity P_{max} , the domain-integrated phytoplankton population M_p at equilibrium does not monotonically decrease with increasing river discharge. The reason for this is that, although bloom intensity slightly declines under higher river discharge, the location of bloom shifts downstream where the width of the estuary is larger.

The stabilisation time T_s (green line in Fig. 8(b)) varies non-monotonically with \tilde{Q} . Overall, it takes less time for the system to reach the steady state for either $\tilde{Q} \leq \tilde{Q}_l$ or $\tilde{Q} \geq \tilde{Q}_h$, compared to the cases $\tilde{Q}_l \leq \tilde{Q} \leq \tilde{Q}_h$. For the low river discharges, initially M_p exhibits a rapid (approximately exponentially) growing phase, whose duration is presented by the inflection times T_i (red line in Fig. 8(b)). Clearly, T_i increases with \tilde{Q} . This implies that the bloom occurs later in time as river discharge increases.

According to the different behaviours of M_p , P_{max} , T_i and T_s for each river discharge, three regimes are identified from the above sensitivity study. The first is the low discharge regime ($0 < \tilde{Q} \leq \tilde{Q}_l$) that is characterised by rapid and intense bloom formation. The second is the moderate discharge regime ($\tilde{Q}_l \leq \tilde{Q} \leq \tilde{Q}_h$), in which population increases significantly slower compared to the low discharge regime. The third is the high discharge regime ($\tilde{Q} \geq \tilde{Q}_h$), characterised by rapid system adjustment and no bloom formation.

In addition, to demonstrate the dimensionless river discharge \tilde{Q} is viable to indicate different regimes, a sensitivity study of bloom dynamics to river discharge was conducted, in which the river discharges Q , maximum specific growth rate μ_{max} and mortality rate m were doubled such that $\tilde{Q} = \frac{Q/V}{\mu_{max} - m} = \frac{(2 \times Q)/V}{2 \times (\mu_{max} - m)}$. The three regimes occur, although the values for \tilde{Q}_l and \tilde{Q}_h are slightly different (results not shown here). This is because other parameters play a role as well (e.g. density-driven flow, horizontal mixing). The new sensitivity study suggests that \tilde{Q} is a reliable parameter to indicate phytoplankton bloom characteristics in eutrophic, vertically well mixed estuaries.

4. Discussion

In this section, the mechanism responsible for the bloom pattern is explained (Section 4.1), as well as the reason why three regimes occur (Section 4.2). The influence of the domain configuration on model results are discussed in Section 4.3 and limitations of the model is discussed in Section 4.4.

4.1. Mechanisms controlling bloom characteristics

To gain insight into the mechanisms that underly the bloom characteristics, the contributions of different terms that affect the growth of P are quantified. This is done by rewriting Eq. (2) as

$$\frac{1}{P} \frac{\partial P}{\partial t} = \underbrace{\frac{[\mu(N, I) - m]}{\mu_{net}}}_{\text{net specific growth rate}} + \underbrace{\frac{1}{P} \left[-v \frac{\partial P}{\partial z} - w \frac{\partial P}{\partial z} - u \frac{\partial P}{\partial x} + \frac{\partial}{\partial z} \left(\kappa_v \frac{\partial P}{\partial z} \right) + \frac{1}{b} \frac{\partial}{\partial x} \left(b \kappa_h \frac{\partial P}{\partial x} \right) \right]}_{\Psi: \text{net accumulation due to non-local processes}}. \quad (15)$$

The left-hand side represents the total growth rate of P at a fixed position. In the first step towards understanding the results, the terms on the right-hand side are categorised into two terms: μ_{net} related to local processes (specific growth and loss) and Ψ related to non-local processes. The latter results from sinking, advection and mixing. All terms have units of day^{-1} .

Fig. 9(a) shows the total growth rate of phytoplankton near the water surface. During the first few days, the total growth rate is negative in the upper reach and positive in the middle reach. Consequently, the along-channel population density maximum forms in the middle reach, as is depicted in Fig. 7(a). The net accumulation due to non-local processes Ψ (Fig. 9(b)) is always negative and opposes the net specific growth rate μ_{net} (Fig. 9(c)). Particularly, during the first 3 days, the

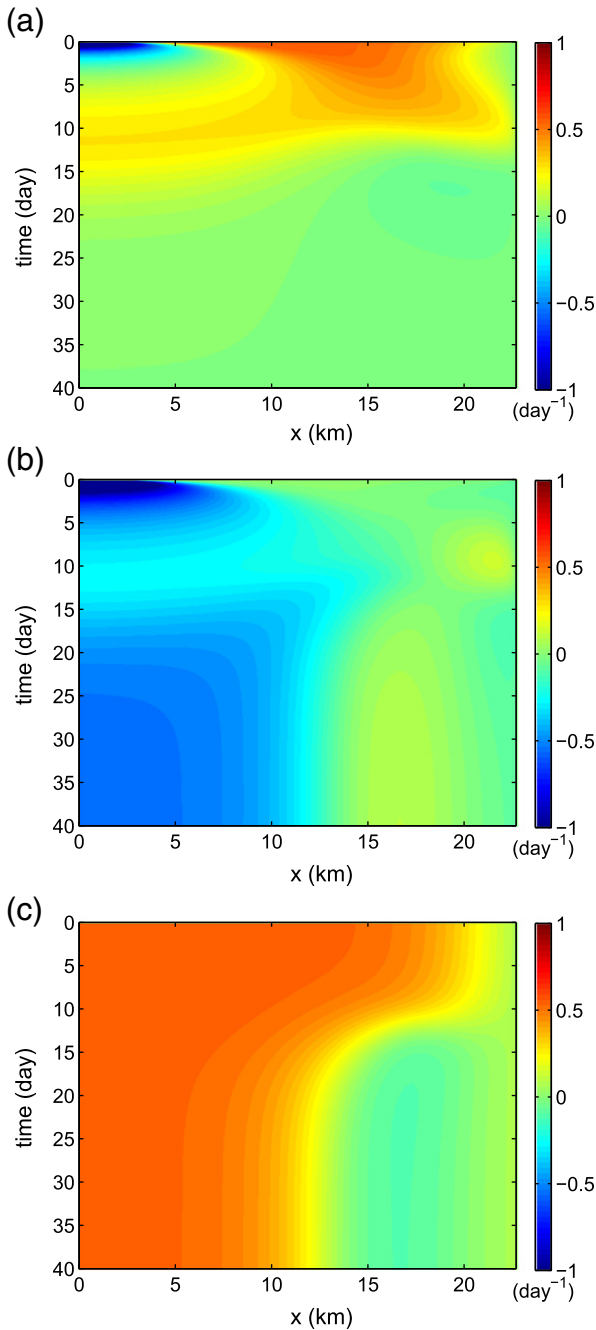


Fig. 9. (a) Contour plot of the total growth rate near the surface for the reference case as a function of x (distance to the river head) and time t . The total growth rate consists of (b)—the net specific growth rate μ_{net} and (c)—the net accumulation due to non-local processes Ψ . Both μ_{net} and Ψ are defined in Eq. (15).

former largely exceeds the latter in the upper reach, which causes the negative total growth rate in this area.

The contribution Ψ to the total growth rate has five constituents related to longitudinal advection, longitudinal diffusion, vertical advection, vertical diffusion and sinking, respectively (see Eq. (15)). The along-channel profiles of these constituents in Ψ at the end of the first day are shown in Fig. 10. Clearly, the longitudinal advection is the leading term that results in the negative contribution to the total growth rate in the upper reach. Recall that the flow is mainly driven by river discharge in the upper reach (Fig. 5). Thus, it is the advection of phytoplankton by river-driven flow that results in the low population density in the upper reach. Here, the longitudinal and vertical mixing tend to smooth the longitudinal gradient of P caused by advection of

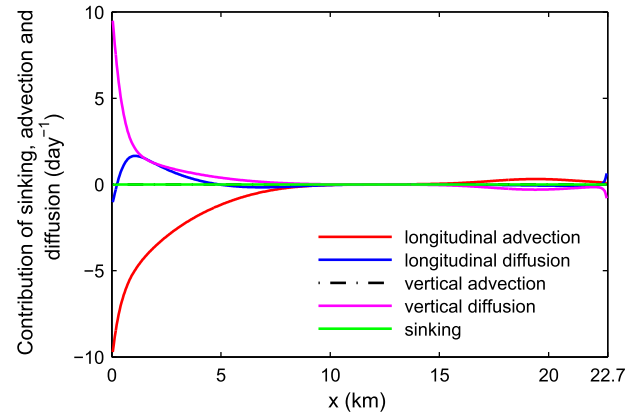


Fig. 10. The constituents of net accumulation due to non-local processes Ψ at the end of the first day (in simulation), where x is distance to the river head.

population by river flow. It should be noted that the river flow also advects nutrient downstream to the middle and lower reach of the estuary, which benefits the growth of phytoplankton. However, this increase in the net specific growth rate μ_{net} does not compensate the negative contribution of longitudinal advection to the total growth rate. This is also illustrated in Fig. 6, where an intense, upper-reach located bloom occurs when the river flow is switched off.

Since the loss rate m is a constant, variations in the net specific growth rate μ_{net} are due to variations in specific growth rate $\mu(N, I)$. The latter is limited by nutrient availability near the water surface as light intensity is high in this area. In the second week, when nutrient is still abundant in the estuary, the total growth rate is positive in the whole domain (Fig. 9(c)). This is consistent with the rapid increase in population, as is shown in Figs. 6(a) and 7(a). Along with the reproduction of phytoplankton and their consumption of nutrient, the total growth rate decreases and finally becomes zero. Moreover, in the lower reach, the values of μ_{net} are always low compared to μ_{max} because the low nutrient concentration limits phytoplankton growth.

4.2. Sensitivity to river discharge

The origin of the occurrence of three regimes identified from the sensitivity study of phytoplankton bloom dynamics to river discharge is investigated in this section. For this, three representative cases are selected from the three regimes, respectively, and will be discussed and compared.

The reference case, where $\bar{Q} = 0.031$, is representative for the low discharge regime. Fig. 11(a) shows the domain-averaged net specific growth rate $\bar{\mu}_{net}$, the domain-averaged net accumulation due to non-local processes $\bar{\Psi}$, and the domain-averaged total growth rate (which is the summation of $\bar{\mu}_{net}$ and $\bar{\Psi}$) for the reference case. In the first (roughly) two weeks, the positive $\bar{\mu}_{net}$ largely outperforms the negative $\bar{\Psi}$, which leads to the rapid increase in population and the formation of the bloom. This results in large consumption of nutrient, hence $\bar{\mu}_{net}$ decreases as well. After four weeks, $\bar{\mu}_{net}$ and $\bar{\Psi}$ compensate each other and the system attains a steady state, which agrees with the stabilising time for this case (see Fig. 8(b)).

In the case $\bar{Q} = 0.153$ (moderate discharge regime), the total population M_P experiences a constantly slow increase rate and the equilibrium M_P is only about in the same order of magnitude as that at the initial time. In Fig. 11(b) it can be seen that $\bar{\mu}_{net}$ is 30% higher than the maximum of $\bar{\mu}_{net}$ in the reference case, and the high $\bar{\mu}_{net}$ holds for the entire evolution period. The reason is that nutrient concentration in the middle and lower reach is higher because larger amount of nutrient is

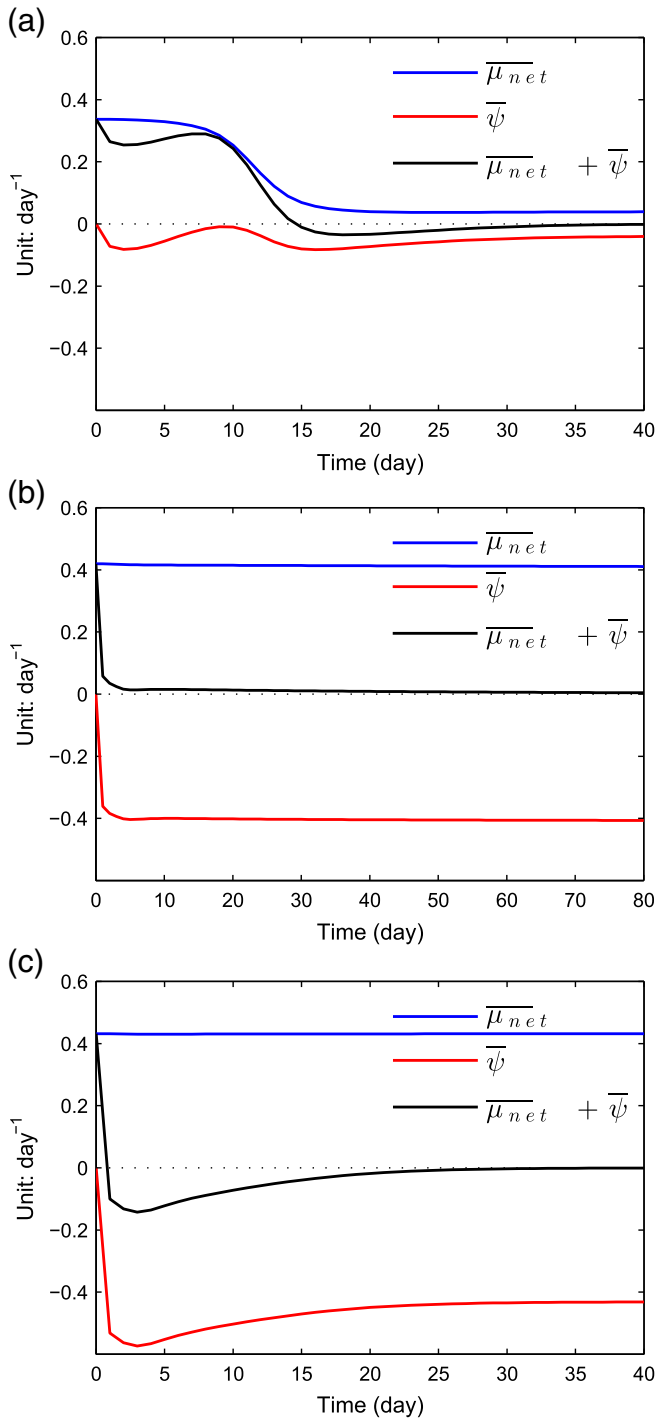


Fig. 11. The domain-averaged specific growth rate $\overline{\mu_{net}}$, the net accumulation due to non-local processes $\overline{\psi}$ and the total growth rate ($\overline{\mu_{net}} + \overline{\psi}$) for the cases: (a): $\tilde{Q} = 0.031$ ($Q = 10 \text{ m}^3 \text{ s}^{-1}$) in the low discharge regime, (b): $\tilde{Q} = 0.153$ ($Q = 50 \text{ m}^3 \text{ s}^{-1}$) in the moderate discharge regime and (c): $\tilde{Q} = 0.215$ ($Q = 70 \text{ m}^3 \text{ s}^{-1}$) in the high discharge regime.

transported into the estuary compared to the low discharge regime. In this case, $\overline{\psi}$ is about 5 times as large as that in the reference case. Due to increased river discharge, phytoplankton remain for a shorter time in high nutrient environment, as they are more quickly advected downstream to the lower nutrient area. The resulting total growth rate ($\overline{\mu_{net}} + \overline{\psi}$) is significantly lower than that in the low discharge regime and becomes even lower after 10 days. Thus, the system takes a

long period (roughly 100 days as shown in Fig. 8(b)) to reach the equilibrium.

In the third case ($\tilde{Q} = 0.215$, i.e. the high discharge regime), the equilibrium M_P is almost the same as that in the initial state (Fig. 8(b)). Both $\overline{\mu_{net}}$ and $\overline{\psi}$ show larger (absolute) values in this case (Fig. 11(c)). Although the increased nutrient amount in the estuary interior allows for even faster growth of phytoplankton compared to the two previous regimes, the negative growth rate contributed by non-local processes constantly outperforms the positive net specific growth rate of phytoplankton, except for a short initial time period. Consequently, M_P hardly increases and no bloom forms in this case.

In marine environments, often Sverdrup theory is used to indicate the possible formation of phytoplankton blooms (Sverdrup, 1953; Platt et al., 1991). This theory states that blooms form if the depth of the surface mixed layer is smaller than the critical depth, i.e. the depth at which local growth rate of phytoplankton becomes smaller than its mortality rate. In the present study, where eutrophic estuaries are considered, Sverdrup theory is not straightforwardly applicable. In the medium and high discharge regimes ($\tilde{Q} \geq \tilde{Q}_I$), the depth of the mixed layer (which equals the depth of water column) is always smaller than the critical depth due to the sufficient nutrient and light availability in such eutrophic shallow estuaries. In spite of this, no bloom forms in these regimes. As revealed by Lucas et al. (1998), this is because the time scale of local net growth of phytoplankton is (much) smaller than that of the flushing (leakage) of phytoplankton by river flow. Instead, the behaviour of phytoplankton dynamics for the medium and high discharge regimes are better illustrated with the theory of Lucas et al. (2009): when the transport time scale is less than the time scale of growth, phytoplankton lack the opportunity to grow on the time scale that they are being transported through this region. For the low discharge regime ($\tilde{Q} \leq \tilde{Q}_I$), in which the time scales of flushing and of horizontal mixing are much larger than that of the local growth of phytoplankton, the Sverdrup bloom theory applies.

4.3. Sensitivity to other estuarine configurations

The three regimes and the values of parameter \tilde{Q}_I and \tilde{Q}_h , which mark the transitions between regimes, are identified based on the results for the geometrical setting of the Taw estuary. It is not clear if the three regimes are present for other estuarine configuration, and how does the estuarine configuration affect the values of \tilde{Q}_I and \tilde{Q}_h . For this, sensitivity studies of phytoplankton bloom to river discharge were also conducted for different water depth (H) and e -folding length scale of estuarine width convergence (L_b). Note that b_0 was tuned along with the change of L_b to keep the water surface area fixed.

Fig. 12 shows the dependences of bloom intensity P_{max} and its location on \tilde{Q} for different H and L_b . Clearly, also for these settings, the three regimes occur. However, quantitative differences exist among these scenarios. First, the bloom intensity weakens if the water depth becomes larger. This is because the depth-averaged light intensity decreases as the water column becomes deeper, which results in a lower depth-averaged growth rate. Second, the bloom location shifts landward as the water depth increases, which is a result of the declined flushing by river flow. With increasing L_b , that is the estuary becomes less convergent, the bloom slightly intensifies and shifts landward. This is because the magnitude of river flow decreases in the upper reach for the less convergent estuary when the water surface area is fixed.

The values for \tilde{Q}_I and \tilde{Q}_h are marked in Fig. 12 for each scenario. It is clear that these values slightly differ among these estuarine configurations. This suggests that the dimensionless parameters \tilde{Q}_I and \tilde{Q}_h are site-specific indicators for the transitions between the regimes. Specifically, \tilde{Q}_I and \tilde{Q}_h increases with L_b . When water depth increases, \tilde{Q}_I decreases. However, there seems no monotonic tendency in the variation of \tilde{Q}_h when water depth changes. This is because, when increasing

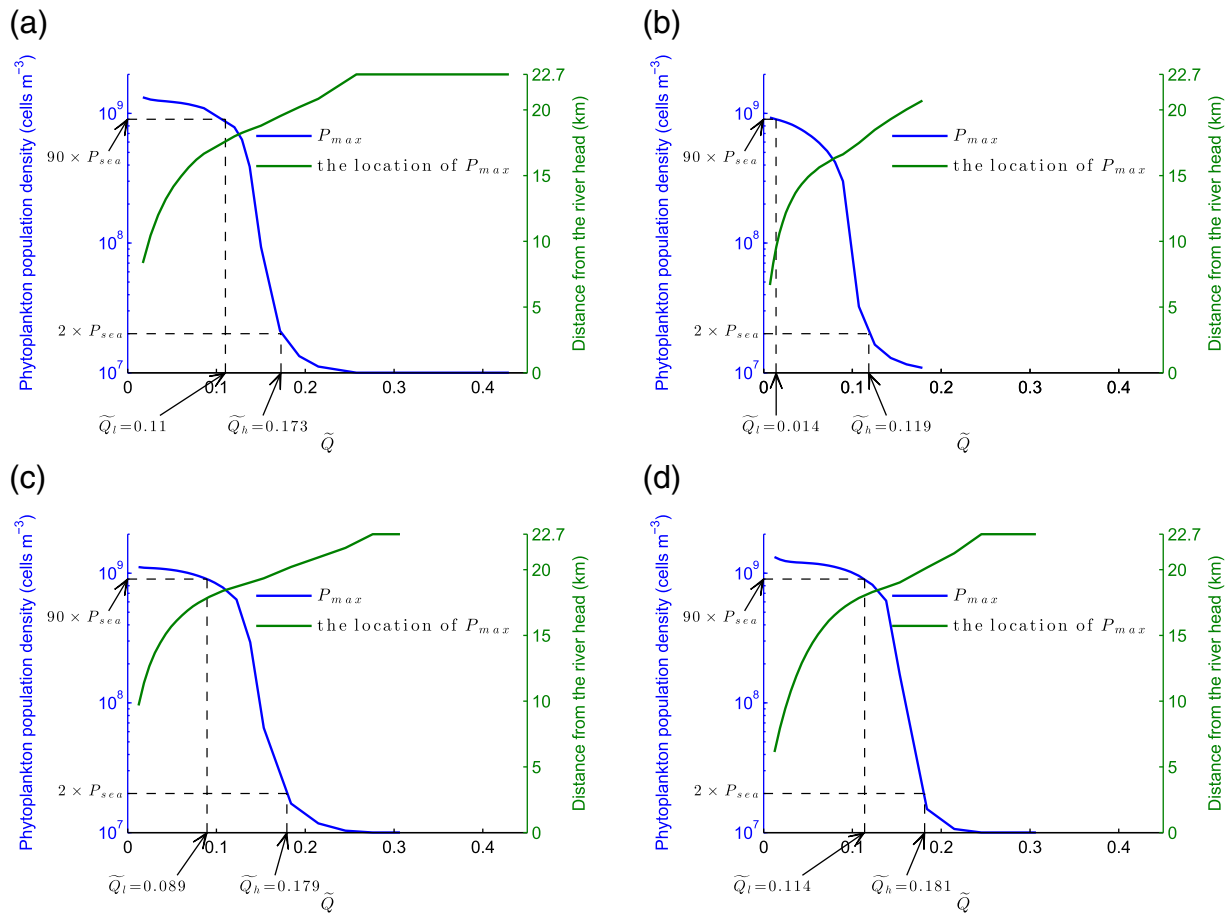


Fig. 12. Blue lines depict bloom intensity P_{max} at equilibrium for different dimensionless river discharges \tilde{Q} , and green lines show the along-channel location of P_{max} . The upper panels are results for water depth $H = 5$ m and 12 m, the lower panels for e -folding length scale $L_b = 4.3$ km and 6.3 km. The values of \tilde{Q}_l and \tilde{Q}_h are marked for each scenario. In the default setting, $\tilde{Q}_l = 0.105$ and $\tilde{Q}_h = 0.181$.

the depth, the flushing of phytoplankton by river flow decreases and the depth-averaged growth rate decreases at the same time.

4.4. Model limitations

Several assumptions and simplifications were imposed to the idealised model, which has reduced the complexity of the problem. The fact that the model captures the observed phytoplankton behaviour in the Taw estuary justifies the rationality of these assumptions and simplifications. However, some assumptions should be relaxed when applying the model to other regions and problems.

First, the water depth is kept constant for the entire estuary and also for all the river discharge cases. It has been reported by Arndt et al. (2007) that the chlorophyll a concentration declines due to the high water volume when the river discharge increases. Also it has been found that water depth affects processes such as depth-dependent friction and further influences sub-tidal flow (Donker and De Swart, 2013). Besides, tidal flats are excluded by taking the constant water depth. The exchange of phytoplankton biomass between tidal flats and main channels of estuaries might affect bloom formation in both compartments as was found by May et al. (2003) for a column model (no variations in along-estuary direction). Although the constant depth is a highly simplification for realistic estuaries, this assumption facilitates the employment of analytical solutions for hydrodynamic processes, which allows for easier control and interpretation of the model results.

Second, tides are only implicitly considered as the source of turbulent mixing. So processes like net transport of phytoplankton by tidal

currents and net transport resulting from variations in water level elevation are not taken into account. Moreover, eddy viscosity and eddy diffusion coefficients in estuaries are generally complex functions of both space and time (Gregg, 1989), where the time-dependence is largely due to tides. In particular, an increase in density stratification reduces the intensity of mixing (Munk and Anderson, 1948) and also affects the vertical distribution of the mixing coefficients (Geyer et al., 2000; Jay and Musiak, 1996). Such changes have a direct impact on the temporal and spatial patterns of phytoplankton (Roegner et al., 2011). Moreover, processes like tidal straining of the density field result in time-varying mixing that (through correlation with tidal shear) drives subtidal flow (Burchard and Schuttelaars, 2010, 2012; Cheng et al., 2010, 2013; Stacey et al., 2010) which causes additional transport of phytoplankton and nutrients.

As mentioned in the Introduction, variability in river discharge causes changes not only in nutrient supply, but also in suspended sediment concentration and stratification in the water column, which were not considered in this study. However, it has been reported by other studies that suspended sediment can strongly influence the phytoplankton production (e.g. (May et al., 2003; De Swart et al., 2009)). These issues discussed above will be taken into account in future research.

5. Conclusions

A two dimensional vertical model that couples physical and biological processes was presented and applied in the Taw estuary to analyse

the responses of the estuarine phytoplankton bloom dynamics to different long-lasting river discharges. This was done by fulfilling two research aims: (1) to demonstrate the importance of flushing of phytoplankton by river flow in formation of observed blooms in eutrophic estuaries; (2) to quantify the dependence of the key characteristics in phytoplankton bloom dynamics on the magnitude of river discharge.

The new model was able to capture the main features of the observed bloom. The timing of the simulated bloom compared well with that of the observation and the spatial pattern was resolved as well. The spatial distribution is characterised by the population density maximum located in the middle reach of the estuary. Here, the role of the river flow is that it advects phytoplankton downstream, thereby suppressing the population density in the upper reach. Moreover, low nutrient availability constrains growth of phytoplankton in the lower reach.

The results of sensitivity study to different river discharges reveal the existence of three distinct regimes. The different outcomes of the competition between growth and advection of phytoplankton explain the differences among the three regimes. The low discharge regime is characterised by rapid formation of intense bloom, the moderate discharge regime by the relatively slow population build-up, and the high discharge regime by the absence of bloom. A bloom forms when the time scale of growth is shorter than that of the advection of phytoplankton by river flow. In contrast, the prevailing advection due to high river flow declines the population and quickly brings the system to the equilibrium. The slow increase of phytoplankton population in the moderate discharge regime is the consequence of the comparable time scales of growth and advection.

Finally, the sensitivity study of phytoplankton bloom dynamics to different river discharges was also carried out for different estuarine configuration. The low, moderate and high discharge regimes also occur in these new scenarios. However, care should be taken when applying this model to real estuaries in reality, as it is based on several strict assumptions.

Acknowledgments

The first author is financially supported by the China Scholarship Council (NO. 201206250039). We thank the editor and the two anonymous reviewers whose inspiring comments has improved the manuscript.

Appendix A. Supplementary data

Supplementary data to this article can be found online at <http://dx.doi.org/10.1016/j.jmarsys.2015.07.007>.

References

- Arndt, S., Vanderborght, J.P., Regnier, P., 2007. Diatom growth response to physical forcing in a macro tidal estuary: coupling hydrodynamics, sediment transport, and biogeochemistry. *J. Geophys. Res.* 112, C05045. <http://dx.doi.org/10.1029/2006JC003581>.
- Arndt, S., Lacroix, G., Gypens, N., Regnier, P., Lancelot, C., 2011. Nutrient dynamics and phytoplankton development along an estuary coastal zone continuum: a model study. *J. Mar. Syst.* 84, 49–66.
- Azevedo, I., Bordalo, A., Duarte, P., 2014. Influence of freshwater inflow variability on the douro estuary primary productivity: a modelling study. *Ecol. Model.* 272, 1–15.
- Behrenfeld, M.J., Boss, E., Siegel, D.A., Shea, D.M., 2005. Carbon-based ocean productivity and phytoplankton physiology from space. *Glob. Biogeochem. Cycles* 19, GB1006. <http://dx.doi.org/10.1029/2004GB002299>.
- Burchard, H., Schuttelaars, H., 2010. Analysis of tidal straining as driver for estuarine circulation in well-mixed estuaries. *J. Phys. Oceanogr.* 42, 261–271.
- Burchard, H., Schuttelaars, H.M., 2012. Analysis of tidal straining as driver for estuarine circulation in well-mixed estuaries. *J. Phys. Oceanogr.* 42, 261–271.
- Cheng, P., Valle-Levinson, A., de Swart, H.E., 2010. Residual currents induced by asymmetric tidal mixing in weakly stratified narrow estuaries. *J. Phys. Oceanogr.* 40, 2135–2147.
- Cheng, P., de Swart, H.E., Valle-Levinson, A., 2013. Role of asymmetric tidal mixing in the subtidal dynamics of narrow estuaries. *J. Geophys. Res.* 118, 2623–2639.
- Cloern, J.E., 1996. Phytoplankton bloom dynamics in coastal ecosystems: a review with some general lessons from sustained investigation of San Francisco Bay, California. *Rev. Geophys.* 34, 127–168.
- Cloern, J.E., Foster, S.Q., Kleckner, A.E., 2014. Phytoplankton primary production in the world's estuarine-coastal ecosystems. *Biogeosciences* 11, 2477–2501.
- Conley, D., 2000. Biogeochemical nutrient cycles and nutrient management strategies. *Hydrobiologia* 410, 87–96.
- Corbett, D., 2010. Resuspension and estuarine nutrient cycling: insights from the Neuse River Estuary. *Biogeosciences* 7, 3289–3300.
- De Swart, H., Schuttelaars, H., Talke, S., 2009. Initial growth of phytoplankton in turbid estuaries: a simple model. *Cont. Shelf Res.* 29, 136–147.
- Diez-Minguito, M., Contreras, E., Polo, M., Losada, M., 2013. Spatio-temporal distribution, along-channel transport, and post-riverflood recovery of salinity in the Guadalquivir Estuary (SW Spain). *J. Geophys. Res.* 118, 2267–2278.
- Donker, J., De Swart, H., 2013. Effects of bottom slope, flocculation and hindered settling on the coupled dynamics of currents and suspended sediment in highly turbid estuaries, a simple model. *Ocean Dyn.* 63, 311–327.
- Dugdale, R., Wilkerson, F., Parker, A., Marchi, A., Taberski, K., 2012. River flow and ammonium discharge determine spring phytoplankton blooms in an urbanized estuary. *Estuar. Coast. Shelf Sci.* 115, 187–199.
- Geyer, W.R., Trowbridge, J.H., Bowen, M., 2000. The dynamics of a partially mixed estuary. *J. Phys. Oceanogr.* 30, 2035–2048.
- Golubkov, M.S., 2009. Phytoplankton primary production in the Neva Estuary at the turn of the 21st century. *Inland Water Biol.* 2, 312–318.
- Gregg, M.C., 1989. Scaling turbulent dissipation in the thermocline. *J. Geophys. Res.* 94 (C7), 9686–9698.
- Hall, N., Pael, H., Peierls, B., Whipple, A., Rossignol, K., 2013. Effects of climatic variability on phytoplankton community structure and bloom development in the eutrophic, microtidal, New River Estuary, North Carolina, USA. *Estuar. Coast. Shelf Sci.* 117, 70–82.
- Hansen, D., Rattray, M., 1965. Gravitational circulation in straits and estuaries. *J. Mar. Res.* 23, 104–122.
- Helder, W., Ruardij, P., 1982. A one-dimensional mixing and flushing model of the Ems-Dollard Estuary: calculation of time scales at different river discharges. *Neth. J. Sea Res.* 15, 293–312.
- Howarth, R., Swaney, D., Butler, T., Marino, R., 2000. Climatic control on eutrophication of the Hudson river estuary. *Ecosystems* 3, 210–215.
- Huisman, J., Thi, N., Karl, D., Sommer, B., 2006. Reduced mixing generates oscillations and chaos in the oceanic deep chlorophyll maximum. *Nature* 439, 322–326.
- Jay, D.A., Musiak, J.D., 1996. Internal tidal asymmetry in channel flows: origins and consequences. *Coast. Estuar. Stud.* 50, 211–249.
- Lucas, L.V., Cloern, J.E., Koseff, J.R., Monismith, S.G., Thompson, J.K., 1998. Does the sverdrup critical depth model explain bloom dynamics in estuaries? *J. Mar. Res.* 56, 375–415.
- Lucas, L.V., Koseff, J.R., Cloern, S.G.M.E., Thompson, J.K., 1999. Processes governing phytoplankton blooms in estuaries. II: the role of horizontal transport. *Mar. Ecol. Prog. Ser.* 187, 17–30.
- Lucas, L., Thompson, J., Brown, L., 2009. Why are diverse relationships observed between phytoplankton biomass and transport time? *Limnol. Oceanogr.* 54, 381–390.
- Maier, G., Glegg, G., Tappin, A., Worsfold, P., 2012. A high resolution temporal study of phytoplankton bloom dynamics in the eutrophic Taw Estuary (SW England). *Sci. Total Environ.* 434, 228–239.
- May, C.L., Koseff, J.R., Lucas, L.V., Cloern, J.E., Schoellhamer, D.H., 2003. Effects of spatial and temporal variability of turbidity on phytoplankton blooms. *Mar. Ecol. Prog. Ser.* 254, 111–128.
- Monismith, S., Kimmerer, W., Burau, J., Stacey, M., 2002. Structure and flow-induced variability of the subtidal salinity field in northern San Francisco Bay. *J. Phys. Oceanogr.* 32, 3003–3019.
- Munk, W., Anderson, E., 1948. Notes on a theory of the thermocline. *J. Mar. Res.* 7, 276–295.
- Peierls, B., Hall, N., Pael, H., 2012. Non-monotonic responses of phytoplankton biomass accumulation to hydrologic variability: a comparison of two coastal plain North Carolina Estuaries. *Estuar. Coasts* 35, 1376–1392.
- Pethick, J., 2007. The Taw-Torridge Estuaries: Geomorphology and Management Report to Taw-Torridge Estuary Officers Group. report. UNESCO Biosphere Reserve.
- Platt, T., Bird, D.F., Sathyendranath, S., 1991. Critical depth and marine primary production. *Proc. R. Soc. B Biol. Sci.* 246, 205–217.
- Popovich, C., Gayoso, A., 1999. Effect of irradiance and temperature on the growth rate of *Thalassiosira curviseriata* Takano (Bacillariophyceae), a bloom diatom in Bahia Blanca Estuary (Argentina). *J. Plankton Res.* 21, 1101–1110.
- Press, W., Flannery, B., Teukolsky, S., Vetterling, W., 1992. Numerical Recipes. Cambridge University Press.
- Roegner, G.C., Seaton, C., Baptista, A.M., 2011. Climatic and tidal forcing of hydrography and chlorophyll concentrations in the Columbia river estuary. *Estuar. Coasts* 34, 281–296.
- Sarthou, G., Timmermans, K., Blain, S., Treguer, P., 2005. Growth physiology and fate of diatoms in the ocean: a review. *J. Sea Res.* 53, 25–42.
- Sin, Y., Wetzel, R., Anderson, I., 1999. Spatial and temporal characteristics of nutrient and phytoplankton dynamics in the York River Estuary, Virginia: analyses of long-term data. *Estuaries* 22, 260–275.
- Stacey, M., Brennan, M., Burau, J., Monismith, S., 2010. The tidally averaged momentum balance in a partially and periodically stratified estuary. *J. Phys. Oceanogr.* 40, 2418–2434.
- Sverdrup, H.U., 1953. On conditions for the vernal blooming of phytoplankton. *ICES J. Mar. Sci.* 18, 287–295.
- Talke, S., De Swart, H., Schuttelaars, H., 2009. Feedback between residual circulations and sediment distribution in highly turbid estuaries: an analytical model. *Phys. Estuar. Coast. Seas* 29, 119–135.
- Warner, J., Geyer, W., Lerczak, J., 2005. Numerical modeling of an estuary: a comprehensive skill assessment. *J. Geophys. Res.* 110, C05001. <http://dx.doi.org/10.1029/2004JC002691>.
- Zakardjian, B.A., Gratton, Y., Vezina, A.F., 2000. Late spring phytoplankton bloom in the Lower St. Lawrence Estuary: the flushing hypothesis revisited. *Mar. Ecol. Prog. Ser.* 192, 31–48.